Global risk of deadly heat

One Sentence Summary: Climatic conditions capable of exceeding human thermoregulatory capacity currently impact almost one third of the world's human population each year with their occurrence projected to increase in step with CO_2 emissions and be aggravated in humid tropical areas.

Camilo Mora[1]†, Bénédicte Dousset[2], Iain R. Caldwell[3], Farrah E. Powell[1], Rollan C. Geronimo[1], Coral R. Bielecki[4], Chelsie W. W. Counsell[3], Bonnie S. Dietrich[5], Emily T. Johnston[4], Leo V Louis[4], Matthew P. Lucas[6], Marie M. McKenzie[1], Alessandra G. Shea[1], Han Tseng[1], Thomas W Giambelluca[1], Lisa R. Leon[7], Ed Hawkins[8], Clay Trauernicht[6]

[1]Department of Geography, Hawai'i at Mānoa, Honolulu, Hawai'i, 96822, USA

[2]Hawai'i Institute of Geophysics and Planetology, University of Hawai'i at Mānoa, Honolulu, Hawai'i, 96822, USA

[3]Hawai'i Institute of Marine Biology, University of Hawai'i at Mānoa, Kāne'ohe, Hawai'i, 96744, USA

[4]Department of Botany, University of Hawai'i at Mānoa, Honolulu, Hawai'i, 96822, USA

[5]Department of Plant and Environmental Protection Sciences, University of Hawai'i at Mānoa, Honolulu, Hawai'i, 96822, USA

[6]Department of Natural Resources and Environmental Management, University of Hawai'i at Mānoa, Honolulu, Hawai'i, 96822, USA

[7]Thermal and Mountain Medicine Division, U.S. Army Research Institute of Environmental Medicine, Natick, Massachusetts 01760, USA

[8] National Centre for Atmospheric Science, Department of Meteorology, University of Reading, Reading, Berkshire, RG6 6BB, UK

†Corresponding author. E-mail: cmora@hawaii.edu

Ongoing climate change can increase the direct risk to human life that occurs when climatic conditions exceed human thermoregulatory capacity (*1-6*). Although there have been numerous reports of increased mortality associated with extreme heat events (*1-7*), quantifying the global risk of heat-related mortality

remains challenging due to a lack of comparable data on heat-related deaths (*2-5*). Here we conducted a global analysis of documented lethal heat events to identify the climatic conditions associated with human death and then quantified the current and projected occurrence of such deadly climatic conditions worldwide. We reviewed papers published between 1980 and 2014, and found 783 cases of excess human mortality associated with heat from 164 cities in 36 countries. Analysis of the climatic conditions of such lethal heat events revealed a global threshold beyond which daily mean surface air temperature and relative humidity become deadly. In agreement with human thermal physiology, the threshold is such that increasing relative humidity decreases the temperatures associated with lethal events. We found that ~30% of the world's population is currently exposed to climatic conditions exceeding this deadly threshold for at least 20 days a year. By 2100, this percentage will increase to ~48% under a scenario with drastic reductions of greenhouse gas emissions and ~74% under a business-as-usual emission scenario. Although tropical areas will not experience the greatest increases in future temperatures, these areas will be exposed to the greatest projected risk to human life from deadly heat because year round high temperature and humidity require a relatively small degree of warming to become deadly. Climatic projections under alternative emissions suggests an almost inevitable increasing threat to human life posed by climate change, which will be greatly aggravated if greenhouse gases are not considerably reduced.

Sporadic heat events, lasting days to weeks, are often related to increased human mortality (*1, 2*), raising serious concerns for human health given ongoing climate change (*1-3, 8-16*). Unfortunately, a number of challenges have hampered global assessments of the risk of heat-related death. First, heat illness (i.e., severe exceedance of the optimum body core temperature) is often underdiagnosed because exposure to extreme heat often results in the dysfunction of multiple organs, which can lead to misdiagnosis (*2, 3, 5, 17*). Second, mortality data from heat exposure are sparse and have not been analyzed in a consistent manner. Here we conducted a global survey of peer-reviewed studies on heat-related mortality to identify the location and timing of past events that caused heat-related deaths. We used climatic data during those events to identify the conditions most likely to result in human death and then quantified the current and projected occurrence of such deadly climatic conditions. Hereafter, we use "lethal" when referring to climatic conditions during documented cases of excess mortality and "deadly" when referring to climatic conditions that could cause death. We make this distinction to acknowledge that climatic conditions which have killed people in the past are obviously capable of causing death but whether or not they result in actual human mortality could be affected by adaptation. We do not quantify human deaths per se because the extent of human mortality will be considerably modified by social adaptation [e.g., use of air conditioning, early warning systems, etc. (*18-20*)]. Although social adaptation could reduce the exposure to deadly heat (*18-20*), it will not affect the occurrence of such conditions. Given the speed of climatic changes and numerous physiological constraints, it is unlikely that human physiology will evolve the necessary higher heat tolerance (*21, 22*), highlighting that outdoor conditions will remain deadly even if social adaptation is broadly implemented. Our aim is to quantify where and when deadly heat conditions occur, which in turn can provide important information on where social adaptation will likely be needed.

We searched available online databases for peer-reviewed publications on heat-related mortality published between 1980 and 2014 (see methods). From over 30,000 relevant references, we identified 911 papers that included data on 1,949 case studies of cities or regions where excess mortality was associated with high temperatures. Case studies were broadly grouped into those focusing on temperature-mortality relationships in a specific city, region, or country (1,166 cases from 273 cities across 49 countries) and those focusing on heat-related mortality during specific episodes (783 cases from 164 cities across 36 countries). Cases were predominantly reported for cities at mid-latitudes, with the highest concentration in North America and Europe (Fig. 1a), and included well-documented heatwaves like those in Chicago in 1995 (~740 deaths, *23*), Paris in 2003 (~4,870 deaths, *24*), Moscow in 2010 (~10,860 deaths, *25*) and many other, less publicized events (list of cases provided at https://rollan.shinyapps.io/HeatwavesMap/). While data on the number of deaths was inconsistently reported, all studies provided information on the place and dates when climatic conditions were lethal, which we used to identify the specific climatic conditions resulting in heat-related mortality.

To identify the climatic conditions related to lethal heat events, we assessed daily climatic data (i.e., surface air temperature, relative humidity, solar radiation, wind speed, and several other metrics, Fig. S1) for lethal heat episodes reported in the literature and an equal number of non-lethal episodes (i.e., periods of equal duration from the same cities but from randomly selected dates); then we used Support Vector Machines (SVM) to identify the climatic conditions that best differentiated lethal and non-lethal episodes. SVMs generate a threshold that maximizes the difference in the attributes of two or more groups allowing to classify objects in either group based on where their given attributes fall with respect to the threshold. In our case, SVM was used to generate a decision threshold that maximizes the difference in climatic conditions of lethal and non-lethal episodes with the conditions on one side of the threshold being lethal and those to the other side being non-lethal (e.g., Fig. 1b). Among all possible pair combinations of the variables analyzed here (Fig. S1-S2), the SVM using mean daily surface air temperature and relative humidity most accurately distinguished between past lethal and non-lethal heat episodes (i.e., 82%, blue line in Fig. 1b); accuracy was measured as the ratio of the number of correctly classified lethal and non-lethal cases to the total number of cases. Adding other variables to the temperature-humidity SVM resulted in less parsimonious SVMs with minimal increases in accuracy (e.g., the SVM model including all 16 variables was only 3% more accurate, Fig. S4). SVM also allows to estimate a classification probability that increases with the distance of an observation to the decision threshold; the use of a 95% probability for the temperature-humidity SVM (red line in Fig. 1b) resulted in 100% accurate predictions of true positives (i.e., only prior lethal heat episodes were on the deadly side of the 95% probability SVM decision boundary). While our analysis used data on local climatic conditions, the resulting pattern between temperature and relative humidity allowed us to accurately classify lethal heat events of different cities from around the world using a single common SVM threshold (Fig. 1b).

The fact that temperature and relative humidity best predict times when climatic conditions become deadly is consistent with human thermal physiology, as they are both directly related to body heat exchange (*2-4*). First, the combination of an optimum body core temperature (i.e., ~37^{o}C), the fact that our metabolism generates heat (~100 W at rest) and that an object cannot dissipate heat to an environment with equal or higher temperature (i.e. the second law of thermodinamics, *22*), dictates that any ambient temperature above 37^{o}C should result in body heat accumulation and a dangerous exceedance of the optimum body core temperature [hyperthermia (5)]. Second, sweating, the main process by which the body dissipates heat, becomes ineffective at high relative humidity (i.e., low water vapor deficit prevents evaporation of sweat); therefore, body heat accumulation can occur at temperatures lower than the optimum body core temperature in environments of high relative humidity. These properties help to explain why the boundary at which temperature becomes deadly decreases with increasing relative humidity (Fig. 1b) and why in our results some heat mortality events occurred at relatively low temperatures (Fig. 1b).

To quantify the global extent of current deadly climatic conditions, we applied the 95% probability SVM decision boundary between mean daily surface air temperature and relative humidity (red line in Fig. 1b, hereafter referred to as deadly threshold) to current global climate data (see Methods). Using data from a climate reanalysis (see methods), we found that in 2000, ~13.2% of the planet's land area, where ~30.6% of the world's human population resides, was exposed to 20 or more days when temperature and humidity surpassed the threshold beyond which such conditions become deadly (Fig. 2, extended results in Fig. S4). Comparatively, using climate simulations for the year 2000 (i.e., historical experiment) developed for the Coupled Model Intercomparison Project phase 5 (CMIP5), we found that ~16.2% (+/-8.3% standard deviation, SD) of the planet's land area, where ~37.0% (+/-9.7% SD) of the world's population resides, was exposed to 20 or more days of potentially deadly conditions of temperature and humidity (results are multimodel medians and standard deviations among Earth System Models; Fig. 2). Both the re-analysis and historical CMIP5 data revealed increasing trends in the area and population exposed to deadly climates during the time period for which such datasets can be compared although the trends in the reanalysis are slightly weaker than in the ESMs (Fig. 2). Overall, there was ~3% mismatch in the area of the planet (~6.4% in global population) between the reanalysis and the multimodel median, and thus, results based on CMIP5 simulations should be interpreted with that error in mind. However, the effects of this mismatch and the uncertainty among Earth System Models were smaller than the predicted changes in deadly days (Fig. S10).

To predict the global extent of future deadly climates, we applied the deadly SVM threshold to mean daily surface air temperature and relative humidity projections from the CMIP5 Earth System Models under low, moderate, and high emissions scenarios (Representative Concentration Pathways, RCPs, 2.6, 4.5, and 8.5, respectively). We found that by 2100, even under the most aggressive mitigation scenario (i.e., RCP 2.6), ~26.9% (+/-8.7% SD) of the world's land area will be exposed to temperature and humidity conditions exceeding the deadly threshold by more than 20 days per year, exposing ~47.6% (+/-9.6% SD) of the world's human population to deadly climates (according to human population projections related to the CMIP5 RCPs, see methods). Scenarios with higher emissions will affect an even greater percentage of the global land area and human population. By 2100, ~34.1% (+/-7.6% SD) and ~47.1% (+/-8.9% SD) of the global land area will be exposed to temperature and humidity conditions that exceed the deadly threshold for more than 20 days per year under RCP 4.5 and RCP 8.5, respectively; this will expose ~53.7% (+/-8.7% SD) and ~73.9% (+/-6.6% SD) of the world's human population to deadly climates by the end of the century (Fig. 2, extended results in Fig. S4).

The projected number of days per year surpassing the deadly threshold increases from mid-latitudes to the tropics (Fig. 5a, Fig S5a,d,g). By 2100, for example, mid-latitudes (e.g., 40° N or S) will be exposed to ~60 deadly days per year compared to almost the entire year in humid tropical areas under RCP 8.5 (Fig. 3b-d, Fig. 4b-d, Fig. 5a). This latitudinal pattern was consistent among all scenarios (Fig. S5a,d,g) and is largely determined by the fact that the number of days with temperatures close to the deadly threshold declines with increasing latitude (i.e., due to greater seasonality; Fig. S6b-d). For example, at mid-latitudes (e.g., New York, Fig. 4i-l) temperatures only approach the deadly threshold during the summer, which represents a smaller proportion of the year; compared to tropical locations (e.g., Jakarta, Fig. 4e-h), which have consistently warm temperatures near the deadly threshold year-round (Fig. S6). Although tropical humid areas will experience less warming than higher latitudes (Fig. 5b, see also *26*), they will be exposed to the greatest increase in the number of deadly days over time, because higher relative humidity in tropical areas requires lower temperatures to cross the deadly threshold (Fig. 4e-h, 5e). Sub-tropical and mid-latitude areas will have fewer days beyond the deadly threshold, but such days will be much hotter in the future (Fig. 4e-h, 5b,d). This general variability in the climatic conditions of deadly days (Fig. 5b-d) is likely related to mean global climate patterns associated with the general circulation of the atmosphere: equatorial convection (i.e., warm, moist air rising) produces high humidity in low latitudes whereas atmospheric subsidence (i.e., cool, dry air sinking) in the subtropics creates low-precipitation, low-humidity zones, where high sensible heat flux contributes to extreme high temperatures (Fig. S5i).

Our study underscores the current and increasing threat to human life posed by climate conditions that exceed human thermo regulatory capacity. Lethal heatwaves are often mentioned as a key consequence of ongoing climate change, with reports typically citing past major events such as Chicago 1995, Paris 2003, or Moscow 2010 (*1-6*). Our literature review indicates, however, that lethal heat events already occur frequently and in many more cities worldwide than suggested by these highly cited examples. Our analysis shows that prior lethal events occurred beyond a general threshold of combined temperature and humidity and that today nearly one-third of the world's population is regularly exposed to climatic conditions surpassing this deadly threshold. The area of the planet and fraction of the world's human population exposed to deadly heat will continue to increase under all emission scenarios, although the risk will be much greater under higher emission scenarios. By 2100, almost three-quarters of the world's human population could be exposed to deadly climatic conditions under high future emissions (RCP 8.5) as opposed to one-half under strong mitigation (RCP 2.6). While it is understood that higher latitudes will undergo more warming than tropical regions (*26*), our results suggest that tropical humid areas will be disproportionately exposed to more days with deadly climatic conditions (Fig. 5a), because these areas have year-round warm temperatures and higher humidity, thus requiring less warming to cross the deadly threshold (Fig. 4, S6). The consequences of exposure to deadly climatic conditions could be further aggravated by an aging population (i.e., a sector of the population highly vulnerable to heat; *2, 3, 4*) and increasing urbanization (i.e., exacerbating heat-island effects; *2, 3, 4*). Our paper emphasizes the importance of aggressive mitigation to minimize exposure to deadly climates and highlights areas of the planet where adaptation will be most needed.

REFERENCES AND NOTES

1. J. A. Patz, D. Campbell-Lendrum, T. Holloway, J. A. Foley, Impact of regional climate change on human health. *Nature* **438**, 310 (2005).
2. R. Basu, J. M. Samet, Relation between elevated ambient temperature and mortality: a review of the epidemiologic evidence. *Epidemiol. Rev.* **24**, 190 (2002).
3. R. S. Kovats, S. Hajat, Heat stress and public health: A critical review. *Annu. Rev. Publ. Health* **29**, 41 (2008).
4. L. R. Leon, *Pathophysiology of heat stroke*. Colloquium Series on Integrated Systems Physiology: From Molecule to Function to Disease (Morgan & Claypool Life Sciences, 2015), vol. 7, pp. 1-101.
5. B. D. Ostro, L. A. Roth, R. S. Green, R. Basu, Estimating the mortality effect of the July 2006 California heat wave. *Environ. Res.* **109**, 614 (2009).
6. J. Glaser *et al.*, Climate change and the emergent epidemic of chronic kidney disease from heat stress in rural communities: The case for heat stress nephropathy. *Clin. J. Am. Soc. Nephrol.*, (2016).
7. J.-M. Robine *et al.*, Death toll exceeded 70,000 in Europe during the summer of 2003. *C. R. Biol.* **331**, 171 (2008).
8. J. Sillmann, E. Roeckner, Indices for extreme events in projections of anthropogenic climate change. *Clim. Chang.* **86**, 83 (2008).
9. G. A. Meehl, C. Tebaldi, More intense, more frequent, and longer lasting heat waves in the 21st century. *Science* **305**, 994 (2004).
10. B. Orlowsky, S. Seneviratne, Global changes in extreme events: regional and seasonal dimension. *Climatic Change* **110**, 669 (2012/02/01, 2012).
11. C. Tebaldi, K. Hayhoe, J. M. Arblaster, G. A. Meehl, Going to the extremes. *Climatic change* **79**, 185 (2006).
12. C. Tebaldi, M. F. Wehner, Benefits of mitigation for future heat extremes under RCP4. 5 compared to RCP8. 5. *Climatic Change*, 1 (2016).
13. A. Sterl *et al.*, When can we expect extremely high surface temperatures? *Geophys. Res. Lett.* **35**, L14703 (2008).
14. C. Huang *et al.*, Projecting future heat-related mortality under climate change scenarios: a systematic review. *Environ. Health Persp.* **119**, 1681 (2011).
15. Y. Guo *et al.*, Global variation in the effects of ambient temperature on mortality: a systematic evaluation. *Epidemiology* **25**, 781 (2014).
16. G. Luber, M. McGeehin, Climate change and extreme heat events. *Am. J. Prev. Med.* **35**, 429 (2008).
17. A. Bouchama, J. P. Knochel, Heat stroke. *New. Engl. J. Med.* **346**, 1978 (2002).

18. J. F. Bobb, R. D. Peng, M. L. Bell, F. Dominici, Heat-related mortality and adaptation to heat in the United States. *Environmental Health Perspectives (Online)* **122**, 811 (2014).
19. A. Gasparrini *et al.*, Temporal variation in heat–mortality associations: a multicountry study. (2015).
20. D. Lowe, K. L. Ebi, B. Forsberg, Heatwave early warning systems and adaptation advice to reduce human health consequences of heatwaves. *Int. J. Env. Res. Public Health* **8**, 4623 (2011).
21. E. G. Hanna, P. W. Tait, Limitations to thermoregulation and acclimatization challenge human adaptation to global warming. *Int. J. Environ. Res. Publ. Health.* **12**, 8034 (2015).
22. S. C. Sherwood, M. Huber, An adaptability limit to climate change due to heat stress. *Proc. Natl. Acad. Sci. USA* **107**, 9552 (2010).
23. S. Whitman *et al.*, Mortality in Chicago attributed to the July 1995 heat wave. *Am. J. Public Health* **87**, 1515 (1997).
24. B. Dousset *et al.*, Satellite monitoring of summer heat waves in the Paris metropolitan area. *Int. J. Climatol.* **31**, 313 (2011).
25. D. Shaposhnikov *et al.*, Mortality related to air pollution with the Moscow heat wave and wildfire of 2010. *Epidemiol.* **25**, 359 (2014).
26. N. S. Diffenbaugh, C. B. Field, Changes in ecologically critical terrestrial climate conditions. *Science* **341**, 486 (2013).
27. B. Jones, B. O'Neill, Spatially explicit global population scenarios consistent with the Shared Socioeconomic Pathways. *Environmental Research Letters* **11**, 084003 (2016).
28. W. Dong, Z. Liu, H. Liao, Q. Tang, X. e. Li, New climate and socio-economic scenarios for assessing global human health challenges due to heat risk. *Climatic Change* **130**, 505 (2015).
29. W. Knorr, A. Arneth, L. Jiang, Demographic controls of future global fire risk. *Nature Climate Change*, (2016).
30. D. Mitchell *et al.*, Attributing human mortality during extreme heat waves to anthropogenic climate change. *Environmental Research Letters* **11**, 074006 (2016).

ACKNOWLEDGMENTS

We thank the Gridded Human Population of the World Database and the National Center for Environmental Prediction and Department of Defense reanalysis database for making their data openly available and Bryan Jones for sharing human population projections. We acknowledge the World Climate Research Programme's Working Group on Coupled Modelling, which is responsible for CMIP5, and thank the climate modeling groups (listed in Table S1) for producing and making available their model outputs. We also thank David Schanzenbach, Sean Cleveland and Ron Merrill from the University of Hawaii Super Computer Facility for allowing access to computing facilities and SeaGrant Hawaii for providing funds to acquire some of the computers used in these analyses. Qi Chen, Adam Smith, Chelsea Dau, Rong Fang, and Sonia Seneviratne, provided valuable contributions to the paper. The opinions or assertions contained herein are the private views of the authors and are not to be construed as official or as reflecting the views of the Army or the Department of Defense.

Fig. 1. Geographical distribution of recent lethal heat events and their climatic conditions. a, places where relationships between heat and mortality have been documented (red points) and where specific heat episodes have been studied (blue points). **b**, mean daily surface air temperature and relative humidity during lethal heat events (black crosses) and during periods of equal duration from the same cities but from randomly selected dates (i.e., non-lethal heat events; red to yellow gradient indicates the density of such non-lethal events). Blue line is the SVM threshold that best separates lethal and non-lethal heat events and the red line is the 95% probability SVM threshold; areas to the right of the thresholds are classified as deadly and those to the left as non-deadly. Support vectors for other variables are shown in Fig. S2.

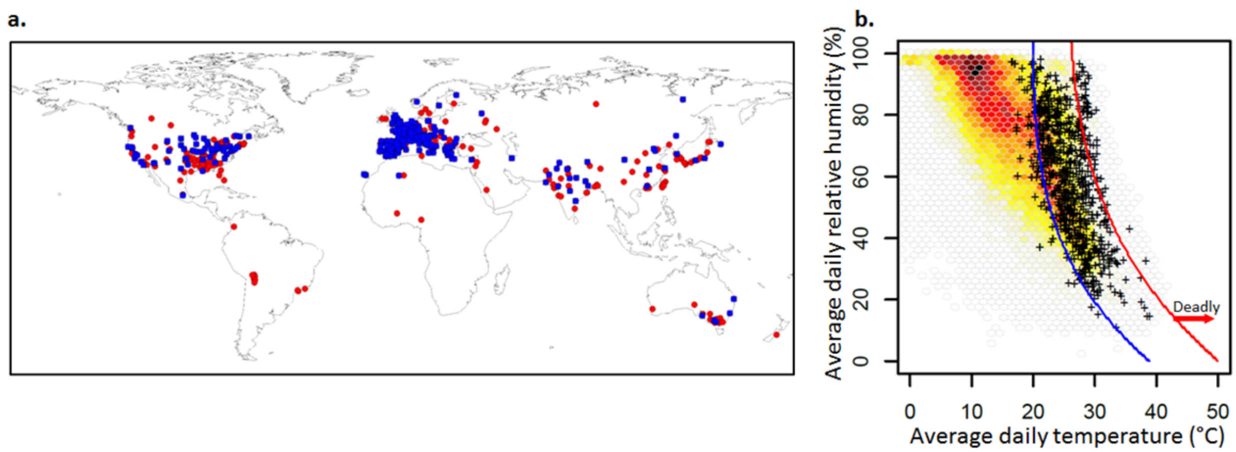

Fig. 2. Current and projected changes in deadly climatic conditions. a, area of the planet and **b,** human population exposed to climatic conditions beyond the 95% SVM deadly threshold (red line in Fig. 1b) for at least 20 days in a year under historical (blue lines), RCP 2.6 (clear blue line), RCP 4.5 (orange lines) and RCP 8.5 (red lines) scenarios. Bolded lines are the multimodel medians, black lines are the results from re-analysis data and faded lines indicate the projections for each Earth System Model. Time series were smoothed with a 10 year average moving window. Area of the planet and human population exposed to different lengths of time are shown in Fig. S4. Results correcting for climatological mean biases between the re-analysis data and each Earth System Model are shown in Fig. S8,S10.

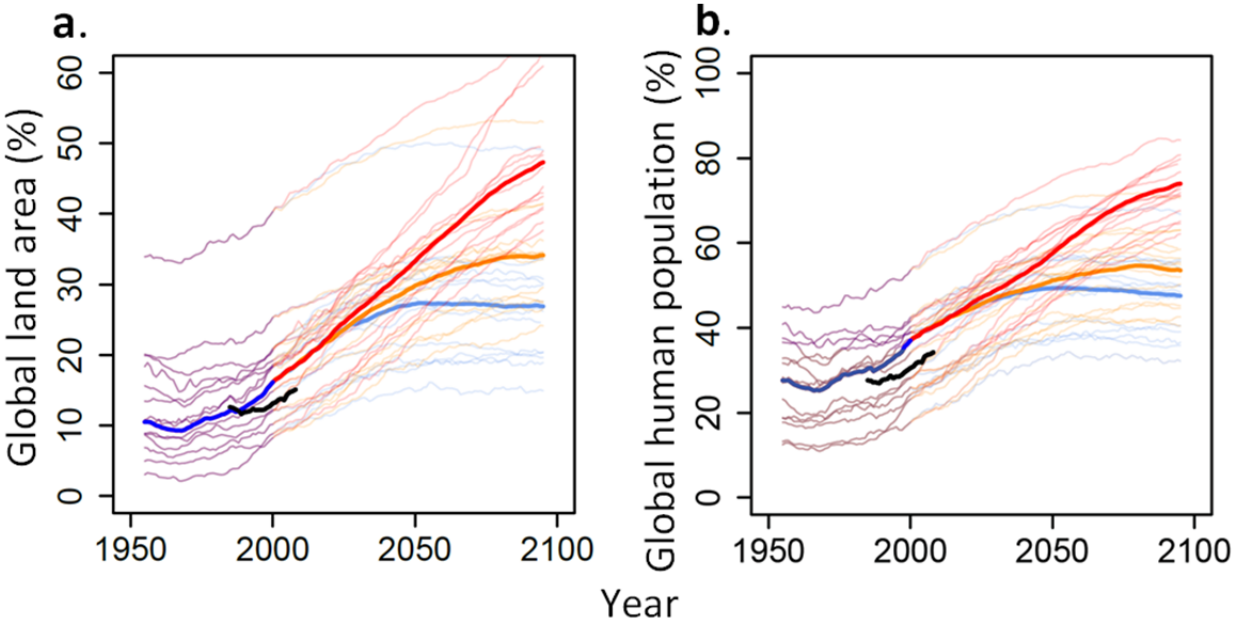

Fig. 3. Geographical distribution of deadly climatic conditions under different emission scenarios. Number of days per year exceeding the threshold of temperature and humidity beyond which climatic conditions become deadly (Fig. 1b), averaged between 1995 and 2005 (**a**, historical experiment) and between 2090 and 2100 under RCP 2.6 (**b**), RCP 4.5 (**c**), and RCP 8.5 (**d**). Results are based on multi-model medians. Grey areas indicate locations with high uncertainty (i.e., the multimodel standard deviation was larger than the projected mean; coefficient of variance >1).

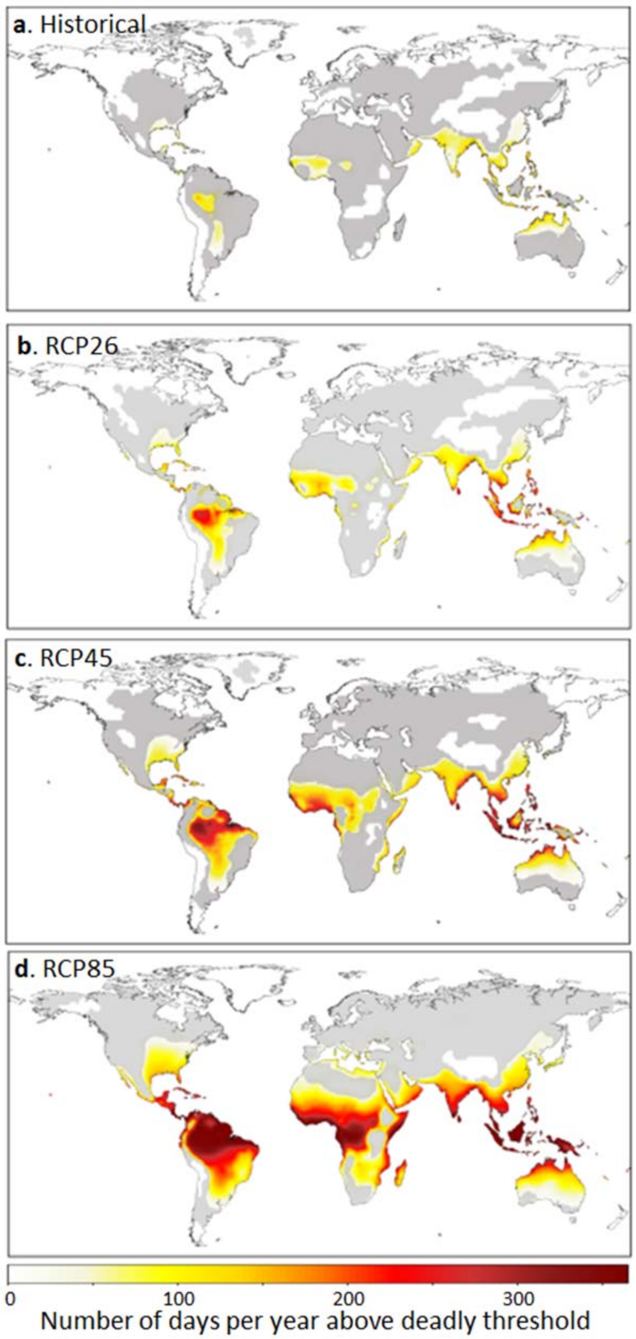

Fig. 4. Latitudinal risk of deadly climates. a-d, distribution of the percentage of days in a given year (i.e., color gradients), at each latitude, as a function of their distance to the deadly threshold (red line in Fig. 1b). Displayed here are the last year in the historical experiment (i.e., 2005; **a**) and the year 2100 under RCP 2.6 (**b**), RCP 4.5 (**c**) and RCP 8.5 (**d**). These plots illustrate that higher latitudes have fewer days near the deadly threshold compared to the tropics. As examples, we show mean temperature and relative humidity for each day in the year 2005 in the historical experiments and the year 2100 for all the RCPs in Jakarta (**e**-**h**) and New York (**i**-**l**), with consecutive days connected by lines. The 95% SVM threshold is shown as a red line with numbers on the upper right hand corner indicating the number of days that cross the threshold and the difference in temperature between 2100 and 2005. Examples are based on a single simulation of a randomly chosen model (i.e., CSIRO-Mk3-6-0).

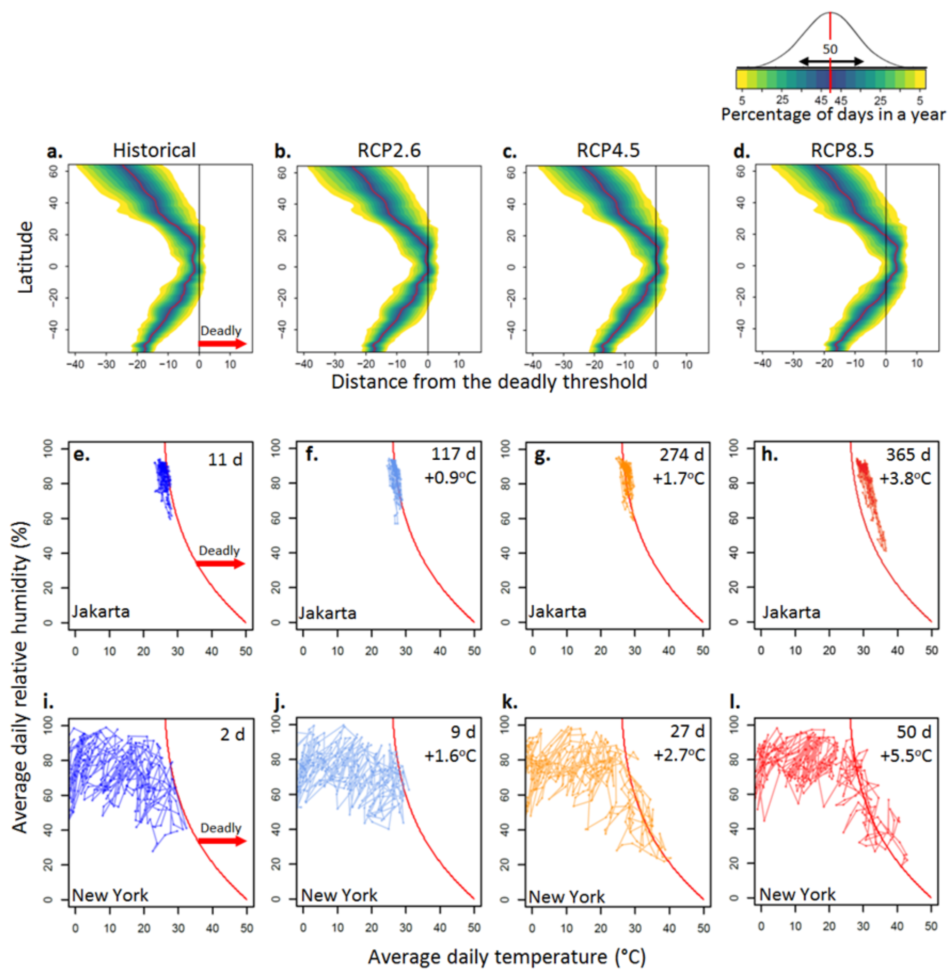

Fig. 5. Simulated spatio-temporal changes in deadly climatic conditions in Earth System Models. a, average changes over time in the number of days per year exceeding the deadly threshold, (**b**) changes in temperature and (**c**) changes in relative humidity during those deadly days, relative to mean value between 1995 and 2005. Plots **d** and **e** show the mean temperature and relative humidity during deadly days, respectively. Results are grouped by latitude and are based on the multimodel medians for the historical experiment, which runs from 1950 to 2005, and RCP 8.5, which runs from 2006 to 2100. Results for all scenarios are shown in Fig. S5.

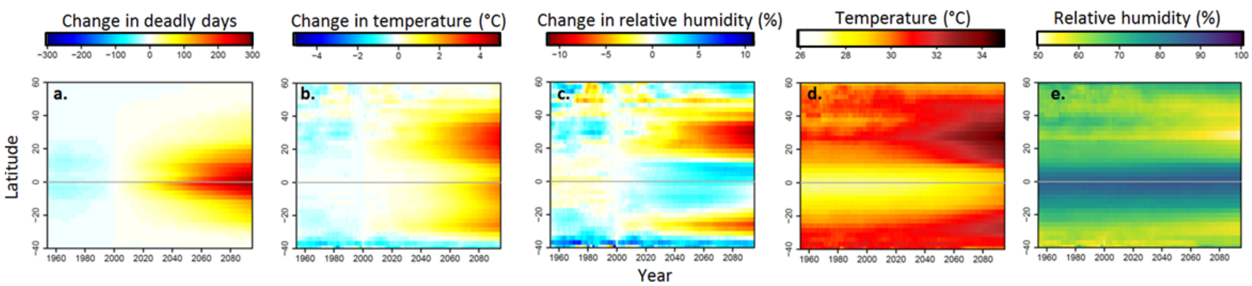

Materials and Methods

Survey of published cases of heat-related mortality. We searched for peer-reviewed studies published between 1980 and 2014 on heat-related mortality in Google Scholar, PubMed, and the Web-of-Science using the following keywords: (human OR people) AND (mortality OR death OR lethal) AND (heat OR temperature). We searched for papers primarily in English but also included papers in Spanish, French, Japanese, and Chinese when found. We reviewed the titles and abstracts of the first 30,000 citations in Google Scholar and all citations from other databases and selected any peer-reviewed publications on heat-related human mortality (we also searched for additional sources in the references). These efforts resulted in 911 peer-reviewed papers from which we collected information on the place and dates of lethal heat events. Several papers noted that human mortality may have occurred beyond the dates in which the extreme climatic conditions occurred; in those cases, we extracted the dates for which the extreme climatic conditions were reported in the given studies. Our goal was to identify the dates in which climatic conditions triggered human mortality regardless of whether mortality was lagged or not.

Climatic conditions related to prior cases of heat related mortality. For the cases in the literature review that reported the place and time of lethal heat events, we assessed information for 16 climatic metrics based on mean daily surface air temperature, relative humidity, solar radiation, and wind speed (Fig. S1). For each of the lethal heat events, we also assessed the same climatic variables for a paired "non-lethal" event of the same duration and from the same city but from a randomly chosen date. Climatic conditions were characterized using daily data from an atmospheric reanalysis of past climate (NCEP-DOE Reanalysis 2). We used the NCEP-DOE Reanalysis database because it is among the most studied and is well characterized relative to newer databases. However, this database is known for biases with respect to coastal winds, so the lack of significance of wind in our analysis should be interpreted with caution. We used Support Vector Machine (SVM) modeling to separate the climatic conditions associated with prior lethal heat events from those associated with non-lethal events. Using SVM, we generated a decision vector/threshold that maximized the distance between lethal and non-lethal episodes with the conditions on one side of the threshold being lethal and those to the other side being non-lethal (e.g., Fig. 1b). We developed such SVM models for all combinations of the variables collected and then compared the accuracy of models to choose the most parsimonious and best performing one.

Projected occurrence of deadly climatic conditions. To quantify the number of days in a year that surpass the threshold beyond which conditions become deadly under alternative emission scenarios, we applied the 95% SVM probability threshold between mean daily surface air temperature and relative humidity of prior lethal heat events to daily climate projections of the same variables. We used the 95% SVM probability threshold because it resulted in a much more accurate classification of prior lethal heat events, and because it restricts projected lethal heat events to much more extreme conditions, hence yielding more conservative results. We used daily climate projections of mean surface air temperature and relative humidity from 20 Earth System Models under four alternative emissions scenarios developed for the recent Coupled Model Intercomparison Project Phase 5 (Table S1). We used the 'historical' experiment, which includes the period from 1950 to 2005 and the Representative Concentration Pathways 2.6, 4.5 and 8.5 (RCP 2.6, 4.5 and 8.5, respectively), which include the period from 2006 to 2100. The historical experiment was designed to model recent climate (reflecting changes due to both anthropogenic and natural causes) and allows the validation of model outputs against available climate observations (Fig. S8-9). RCP pathways represent contrasting mitigation efforts between rapid greenhouse gas reductions (RCP 2.6) and a business-as-usual scenario (RCP 8.5). All analyses were run at the original resolution of each climate database and the results were interpolated to a common 1.5° grid cell size using a bilinear function.

Projections of global land coverage and risk to human populations from deadly climatic conditions. To calculate the amount of land area and fraction of the human population that are likely to be exposed to deadly climates each year, we summed the land area and human population for all cells experiencing varying numbers of days in a year beyond the deadly threshold (Fig. 2, Fig. S4). We used the Gridded Population of the World from the Socioeconomic Data and Applications Center (http://sedac.ciesin.columbia.edu/data/set/gpw-v3-population-count-future-estimates/data-download#) to estimate human exposure up to the year 2005 and human population projections consistent with the different emission scenarios used in the CMIP5 to estimate exposure between 2006 and 2100. For the population projections, we specifically used the spatially explicit global population scenarios consistent with the Shared Socioeconomic Pathways (SSP) developed by Jones et al (*27*), pairing RCP 2.6 with SSP1 (as in *28*), RCP 4.5 with SSP3, and RCP 8.5 with SSP5 (as in *29*).

Limitations

There are several potential limitations to our study. First, the lethality of deadly climatic conditions can be mediated by various demographic (e.g., age structure), socio-economic (e.g., air conditioning, early warning systems) and urban planning (e.g., vegetation, high albedo surface) factors that were not considered in our study. Consideration of these factors would improve the understanding of global human vulnerability to heat exposure and may reduce the number of human deaths, but they are unlikely to affect the occurrence of deadly climatic conditions, which is what we estimated. Second, our survey of cases of heat related mortality was restricted to the period between 1980 and 2014 and any bias or temporal heterogeneity in the monitoring of lethal heatwaves and epidemiological studies in this period may influence the cases we studied and the resulting SVM model. Third, while general agreement among models was found in the predictions of deadly climatic conditions in tropical areas, greater variability among models was seen in such projections at higher latitudes (grey areas in Fig. 3). Because deadly conditions are more rare at higher latitudes (Fig. 4), a larger number of model ensembles might allow for more definitive statements about the risk of deadly climates in such regions, as has been suggested for similar cases of rare events (*30*). Finally, it is possible that some lethal heat events were not documented in peer-reviewed publications and, if the dates of those undocumented events happened to be selected as part of the non-lethal events in our analysis, this could affect the resulting SVM model. However, this error is likely minimal because there is a low probability of randomly selecting such rare and brief events from a 30 year period in the given cities.

Supplementary Table 1. Earth System Models analyzed (Coupled Model Intercomparison Project Phase 5).

CENTER	COUNTRY	MODEL	Historical	RCP2.6	RCP4.5	RCP8.5
Commonwealth Scientific and Industrial Research Organization and Bureau of Meteorology	Australia	Access1.3	✔	-	✔	✔
Beijing Climate Center, China Meteorological Administration	China	BCC-CSM1.1	✔	✔	✔	✔
		BCC-CSM1.1(m)	✔	✔	✔	✔
College of Global Change and Earth System Science, Beijing Normal University	China	BNU-ESM	✔	✔	✔	✔
Canadian Centre for Climate Modelling and Analysis	Canada	CanESM2	✔	✔	✔	✔
Centre National de Recherches Meteorologiques / Centre Europeen de Recherche et Formation Avancees en Calcul Scientifique	France	CNRM-CM5	✔	✔	✔	✔
Commonwealth Scientific and Industrial Research Organization with Queensland Climate Change Centre of Excellence	Australia	CSIRO-Mk3.6.0	✔	✔	✔	✔
Met Office Hadley Centre	UK	HadGEM2-CC	✔	-	✔	✔
Met Office Hadley Centre (additional HadGEM2-ES realizations contributed by Instituto Nacional de Pesquisas Espaciais)	UK	HadGEM2-ES	✔	✔	✔	✔
Institute for Numerical Mathematics	Russia	INM-CM4	✔	-	✔	✔
Institute Pierre-Simon Laplace	France	IPSL-CM5A-LR	✔	✔	✔	✔
		IPSL-CM5A-MR	✔	✔	✔	✔
		IPSL-CM5B-LR	✔	-	✔	✔
Atmosphere and Ocean Research Institute (The University of Tokyo), National Institute for Environmental Studies, and Japan Agency for Marine-Earth Science and Technology	Japan	MIROC4h *	✔	-	✔	
		MIROC5	✔	✔	✔	✔
Japan Agency for Marine-Earth Science and Technology, Atmosphere and Ocean Research Institute (The University of Tokyo), and National Institute for Environmental Studies	Japan	MIROC-ESM	✔	✔	✔	✔
		MIROC-ESM-CHEM	✔	✔	✔	✔
Meteorological Research Institute	Japan	MRI-CGCM3	✔	✔	✔	✔
		MRI-ESM1	✔	-	-	✔
Norwegian Climate Centre	Norway	NorESM1-M	✔	✔	✔	✔

List of models used in this study. We only considered models that provided the complete series of data from 1950 to 2100 for surface downwelling shortwave radiation (rsds), daily-mean near-surface wind speed (sfcWind), daily mean near-surface air temperature (tas), daily minimum near-surface air temperature (tasmin), and daily maximum near-surface air temperature (tasmax).

* Projection ends in 2035.

Fig. S1. Characterization of climatic conditions during heat lethal events. For the place and time of each lethal heat, we calculated 16 climatic variables described below.

1. Mean daily temperature during the days of the event (^{o}C).
2. Mean minimum daily temperature during the days of the event (^{o}C).
3. Mean maximum daily temperature during the days of the event (^{o}C).
4. Mean daily relative humidity during the days of the event (%).
5. Mean daily wind speed during the days of the event (m/s).
6. Mean daily solar radiation during the days of the event (watts/m^2).
7. Cumulative number of degrees Celsius above the 90th percentile during the days of the event, using mean daily temperature (heating degree days, ^{o}C).
8. Same as #7 but using minimum daily temperature.
9. Same as #7 but using maximum daily temperature.
10. Cumulative humidity above the 90th humidity percentile for the period of the heat event.
11. Cumulative wind speed above the 90th wind speed percentile for the period of the heat event.
12. Cumulative solar radiation above the 90th radiation percentile for the period of the heat event.
13. Duration (number of days of the event).
14. Intensity (the largest difference between the mean daily temperature and the 90th temperature percentile, ^{o}C).
15. Time to peak of summer (i.e., number of days between the time of the event and the hottest day in the climatology, in days). Heat episodes that occur close to the peak of the summer are assumed to be dangerous because, in such cases, temperature can exceed the maximum adaptability gained historically during the hottest times of the summer.
16. Absolute temperature change (mean difference between the maximum and minimum daily temperatures during the heat event, ^{o}C). Heat event with small absolute thermal change could be dangerous because high temperatures persisting overnight preclude physiological recovery.

Fig. S2. Support Vector Machine models for pairs of variables analyzed in this study. A total of 16 variables were used in this study to discriminate the climate conditions during days that were lethal and not. Below is a subset of pair-wise models. The accuracy of each SVM is shown inside the plots. Red lines are the SVM thresholds that best separate lethal and non-lethal heat events; shaded red areas indicate the side of the threshold where conditions are classified as deadly. Black points indicate conditions of documented lethal heat events. Red to green gradient indicates the density of non-lethal events. The classification accuracy for all possible combinations of all 16 variables is shown in Fig. S3.

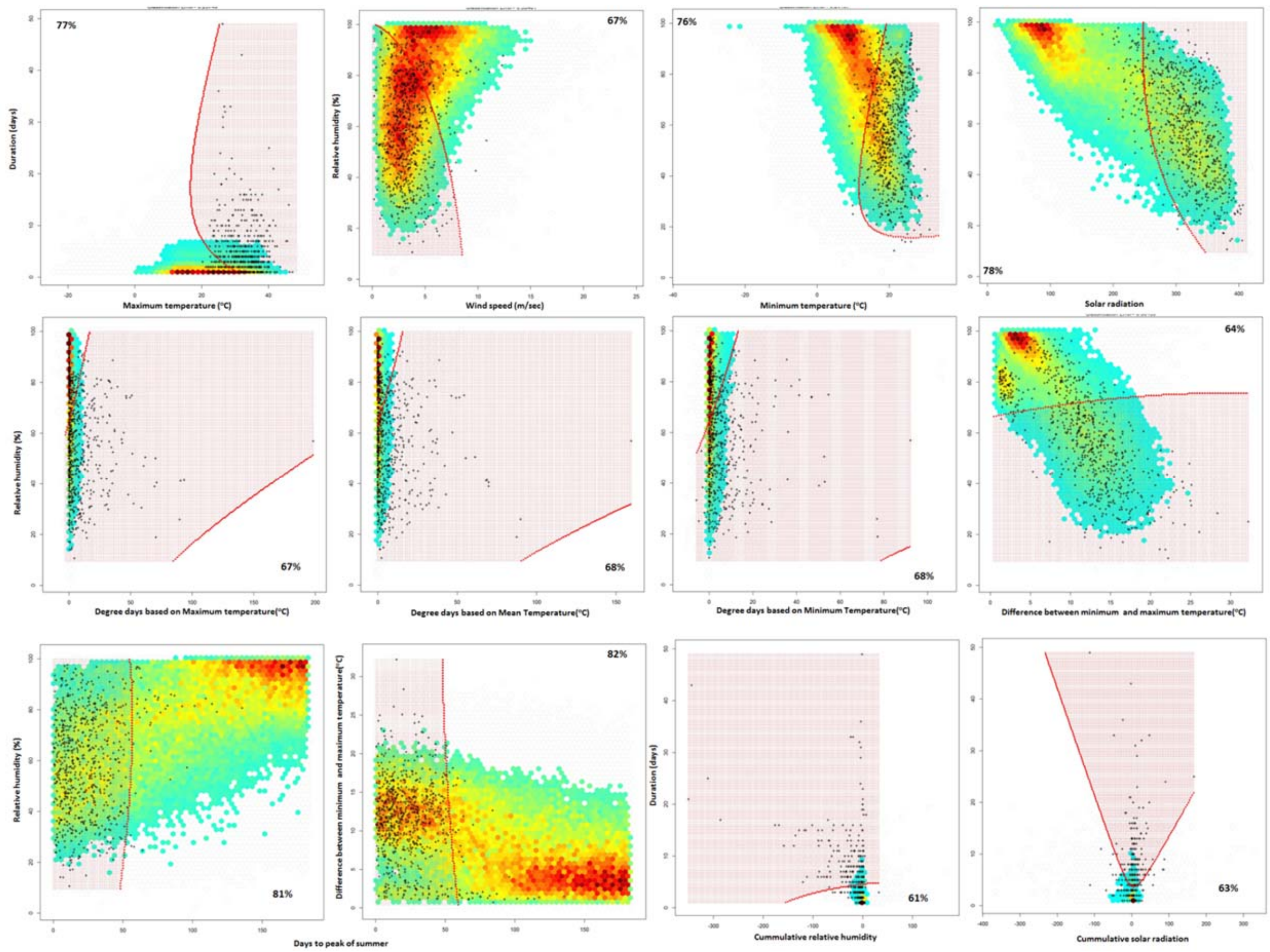

Fig. S3. Improvements in SVM accuracy (i.e., classification error) with increases in the number of variables considered. Black points represent each of the 65,535 potential SVM models resulting from all possible combinations of the 16 climatic variables used in this study. A model with mean daily surface air temperature and mean daily relative humidity yielded an accuracy of 83% (horizontal line in the plot below), which was the highest accuracy of any two pairs of variables. Less parsimonious models increased accuracy only minimally, with the model including all 16 variables improving accuracy by only 3%.

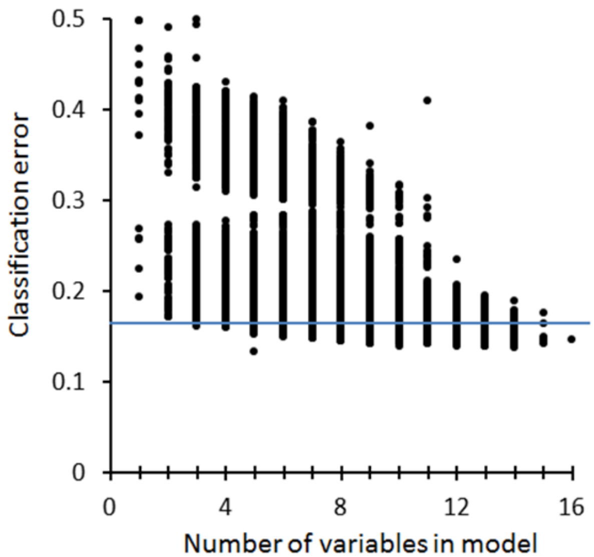

Fig. S4. Current and projected changes in deadly climatic conditions. Extended results of Fig. 2. Plots show the area of the planet and global population exposed to various numbers of days surpassing the deadly threshold.

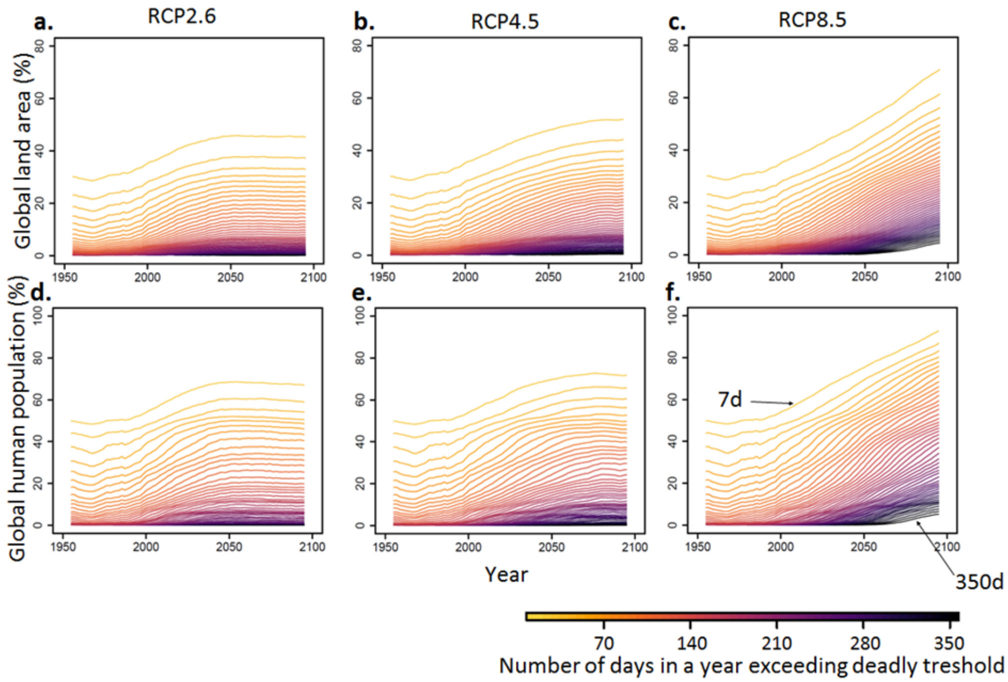

Fig. S5. Spatio-temporal changes in deadly climatic conditions. Extended results of Fig. 5 for each of the RCPs.

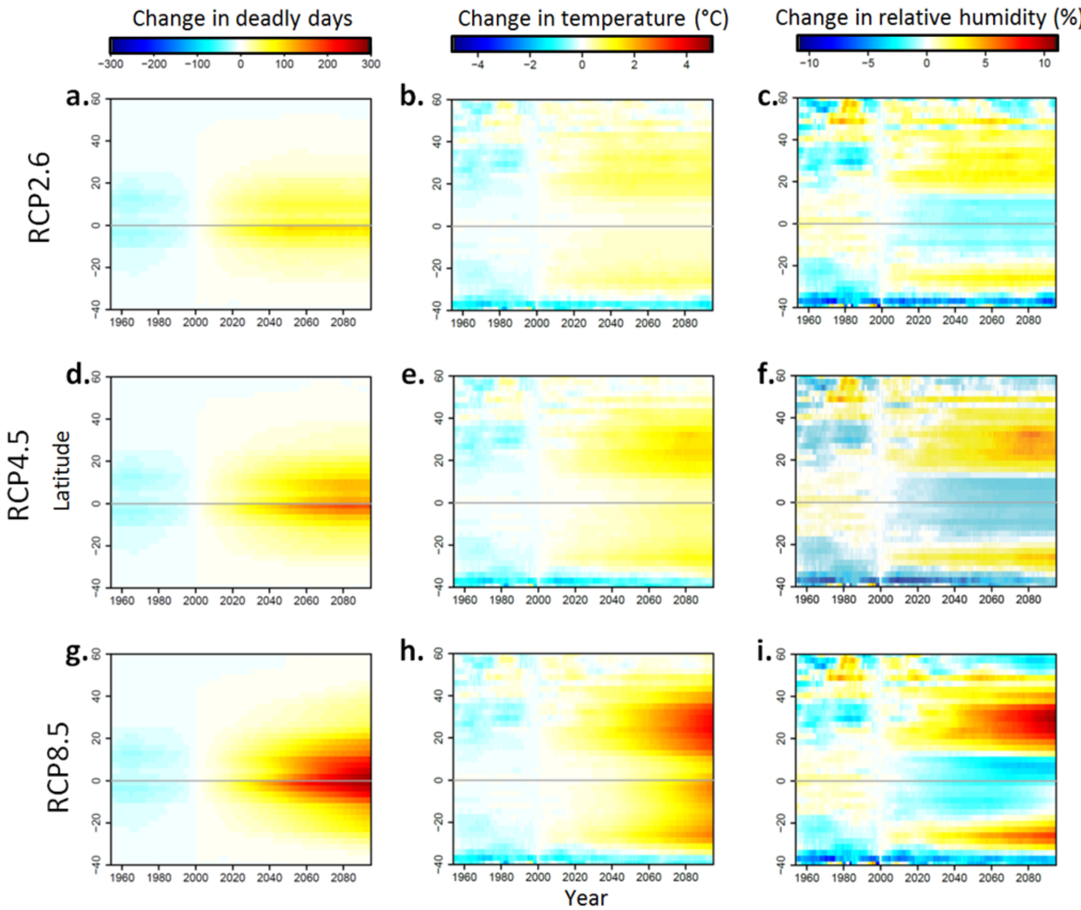

Fig. S6. Proximity of climatic conditions to the deadly threshold by latitude under different RCPs. Distribution of the percentage of days in a given year (i.e., color gradients), at each latitude, as a function of their temperature (**a-d**), relative humidity (**e-h**) and distance to the deadly threshold (**i-l**). Displayed here are the last year in the historical experiment (i.e., 2005; **a**) and the year 2100 under RCP 2.6 (**b**), RCP 4.5 (**c**) and RCP 8.5. Illustrations are based on a randomly chosen model (i.e., CSIRO-Mk3-6-0). Vertical black lines are shown as a guide for comparison among plots.

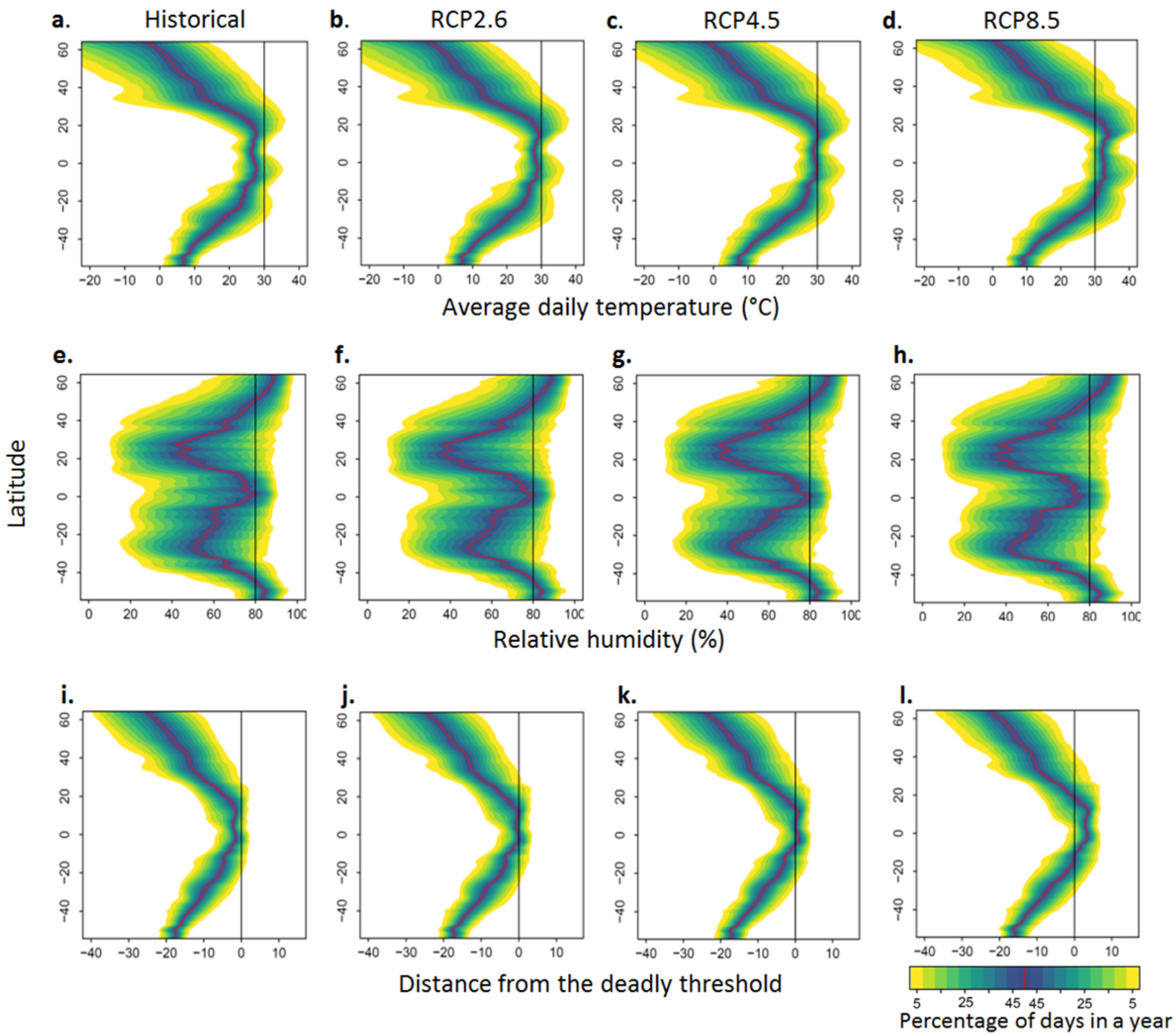

Fig. S7. Possible mechanisms for large scale variations in the conditions of deadly days. Over time the number of deadly days increased most substantially towards the tropics (**a**) despite the less extreme warming there (**b**). Such a reduced warming, however, is accompanied by increases in relative humidity in tropical areas (**c**). Tropical areas have predominantly higher soil moisture in contrast to dry mid-latitudes (**d**). Soil moisture affects the partitioning of energy fluxes (e.g., Bowen ratio: sensible heat/latent heat, **f**), with the lack of moisture availability in dry areas increasing sensible heat flux thus amplifying extreme temperatures (**i**). All plots are based on RCP8.5. Data in plots **f-i** are for the year 2100. Change in temperature in plot **i**, is the absolute difference between 2005 and 2100.

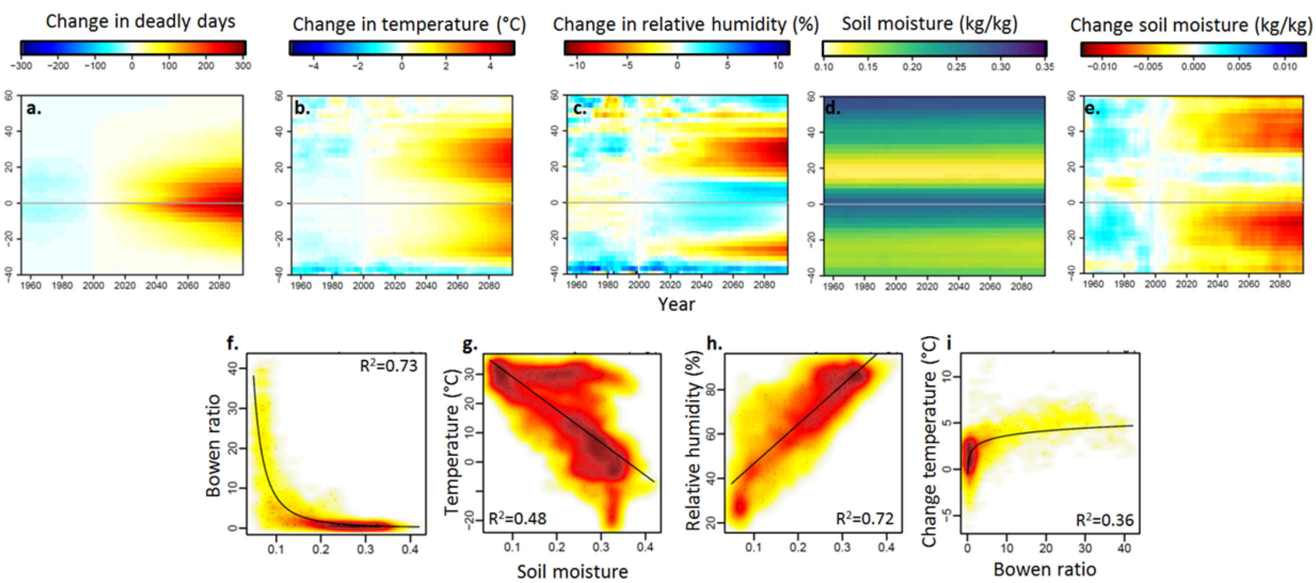

Fig. S8. Effect of climatology bias in Earth System Models in predicting deadly climates. Climatic projections of Earth System Models can be offset from actual climatic values due to variability in the initial parameters used in the model. This bias can affect results based on threshold analyses that rely on absolute values. For instance, consider a model with a 2°C negative bias (i.e., the model simulates 2°C colder than it actually is) and the objective is to assess whether temperature of a given place exceeds a 32°C threshold. If this model simulates a 31°C temperature, the nominal data will indicate that temperature does not exceed the 32°C threshold. However, if the 2°C bias in the model is accounted for, then the expected temperature will be 33°C, which does exceed the 32°C threshold. To assess the effect of climatological biases in Earth System Models, we ran the SVM model based on mean daily temperature and relative humidity with the nominal data from the Earth System Models, and with data that subtracted any bias in the climatology of the two variables. For each variable in the CMIP5 models and NCEP-DOE Reanalysis data from 1980 to 2005, we calculated their climatology (average value) for every global cell for any given day of the year plus and minus two days (a five day window centered in the given day of the year). The climatology from the Earth System Model was subtracted from the climatology of reanalysis data and this "bias" was added to the projected variables for the given cell and time of the year for that given model. In the case of relative humidity, any bias-corrected values above 100% were set to 100%. The results from all CMIP5 models with raw and bias-corrected data were grouped and averaged to create a multi-model average of each type of data. The plots below show the number of days per year above the SVM threshold with the two sources of data for the year 2005 (**a**) , and coefficient of determination (R^2) for every individual year from 1980 to 2005 (**b**). The high similarity between the nominal data and the bias corrected data is probably explained by the fact that the use of a multimodel average can even up biases among models, although it has also been shown that model errors are reduced in analyses that combine temperature and relative humidity (Fig. S10).

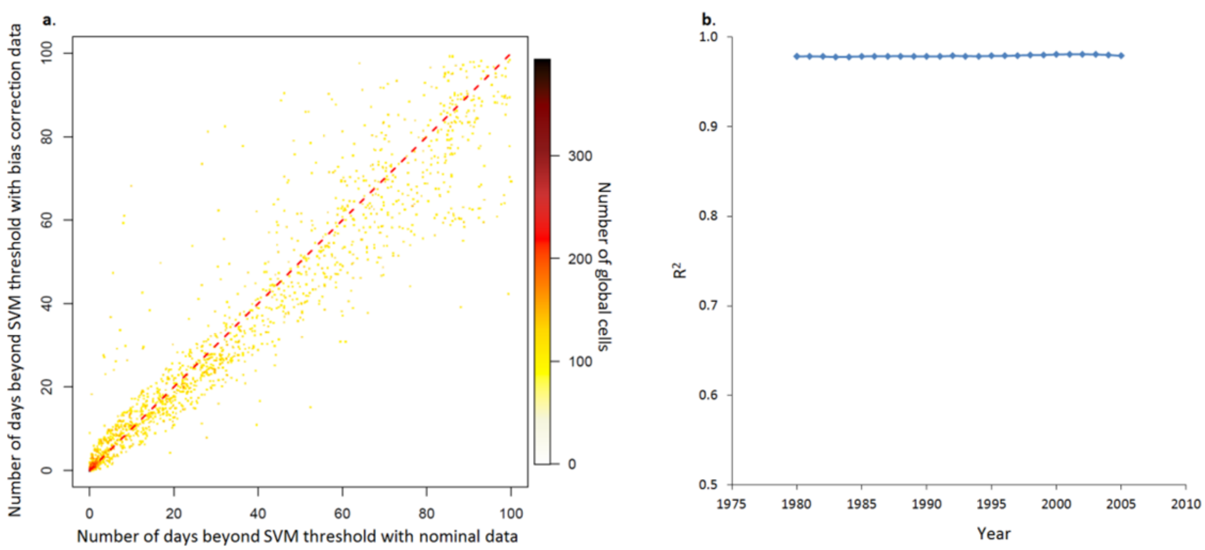

Fig. S9. Comparison of deadly heat anomalies from NCEP-DOE Reanalysis data with individual Earth System Models and their multimodel median. Comparisons of the cumulative number of days beyond the deadly SVM threshold (**a**), and temperature (**b**) and relative humidity (**c**) during those days between each CMIP5 Earth System Model and their multimodel median to the same attributes predicted from the NCEP-DOE Reanalysis data from 1980 to 2005 (the common time frame for both data sources). The Taylor diagrams below compare NCEP-DOE Reanalysis data with CMIP5 model simulations, and summarize three different metrics of similitude: correlation (curved axis), ratio of the standard deviations (x and y axes), and root mean squared error (blue arcs). Blue points indicate perfect fit, red points indicate the multimodel average, and black points indicate the comparison of each Earth System Model to the NCEP-DOE Reanalysis data. The closer a red or black point is to the blue point, the better the fit between reanalysis and simulated data.

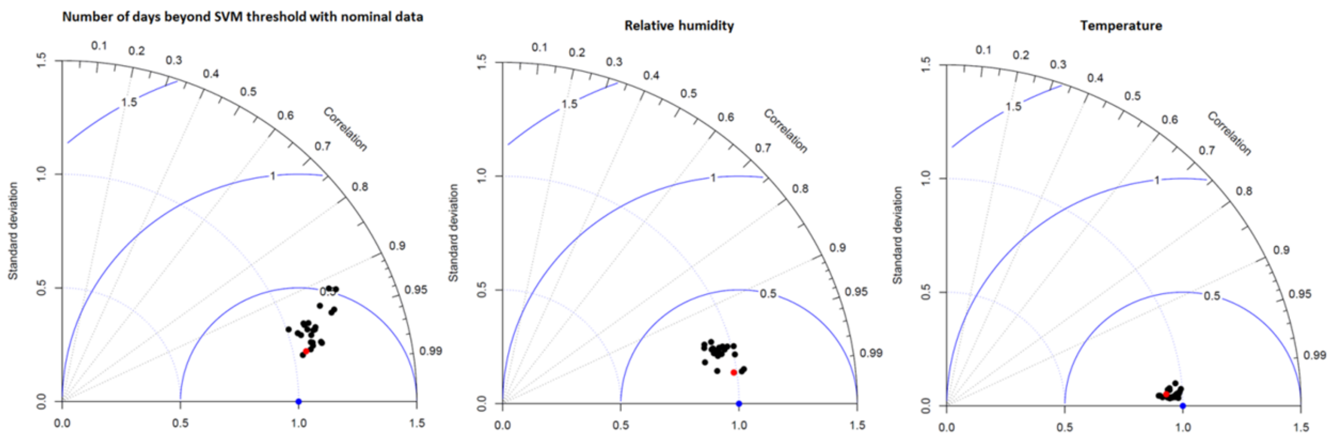

Fig. S10. Potential effects of projection errors in reported trends. Two key sources of error in our analysis are related to the "accuracy" and "precision" with which data from Earth System Model predict the occurrence of deadly climatic conditions. Accuracy can be broadly defined as the extent to which a measurement resembles the true value and precision as the variability among replicated measurements. To quantify accuracy, for each land cell, we calculated the difference between the number of deadly days in a year predicted using the re-analysis data minus the CMIP5 multimodel median for the year 2005. To quantify precision, at each time step for each land cell, we quantified the standard deviation among CMIP5 models in their predictions of the number of deadly days in a year, and divided such a value by the multimodel mean to calculate the coefficient of variance (CV). To assess the extent to which these two sources error affect our results, for each land cell, we subtracted the accuracy error from the multimodel median prediction of the number of deadly days (red-lines in the plots below), independently we also removed any cell with a CV large than 100% (blue lines in the plots below) and in a third test, we removed any cell with CV larger than 100% and for those cells that remained we subtracted the error in accuracy (green lines in plots below). From the resulting data, we calculated the area of the planet and the percent of the global population exposed to more than 20 deadly days in a year as in Fig. 2 of the paper. The analyses were repeated independently for the nominal data and the data correcting for each model's mean climatology bias (see Fig. S8). As noted in the figures below, precision among Earth System models added the largest error in our analysis but even when combined with the errors in accuracy and using nominal or climatology bias correction data, such errors were insufficient to modify the general trends reported here. Several factors may add to this. First, general trends are based on a multimodel median ensemble. Second, results are based on variables that are relatively well predicted by Earth System Models (Fig. S9). Finally, our approach combines temperature and humidity, which are two variables that have been found to yield robust projections when used combined, as their causal interrelation considerably reduces uncertainties (Fischer & Knutti 2013).

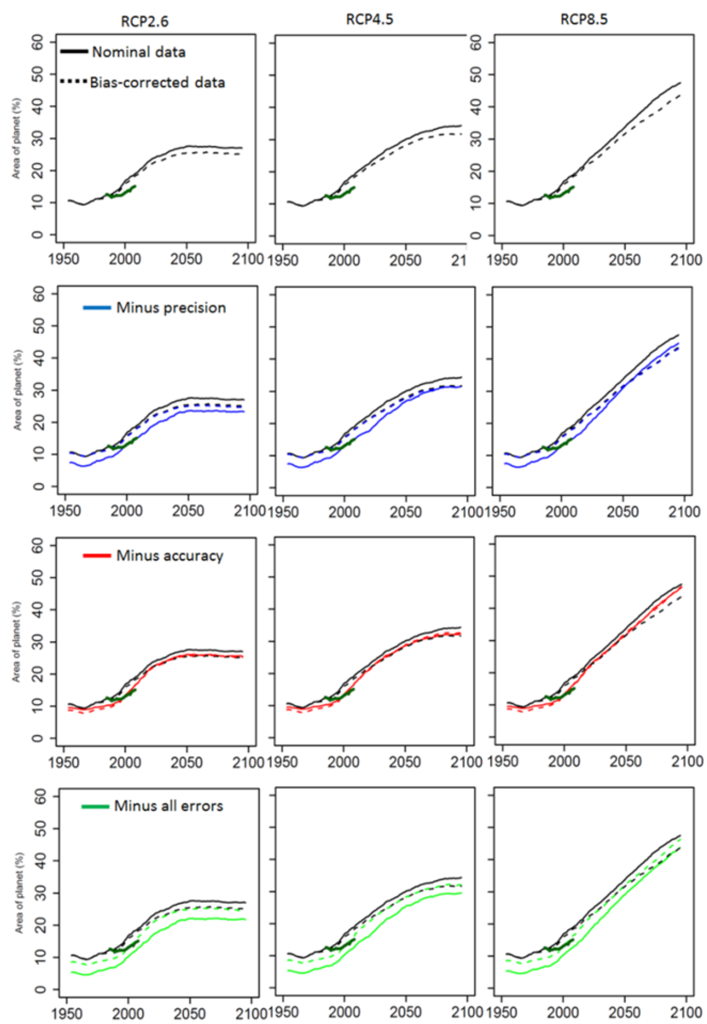

Cont. Fig. S10. Error counting for human population data. Note that the fraction of the world's human population exposed to deadly climates has a slight "jump" around the year 2005, which is related to the shift in the human population databases used. The CIESIN database was used for any climatic projection prior to 2005, whereas the SSP human population projections were paired with the different RCPs after 2006 (see methods).

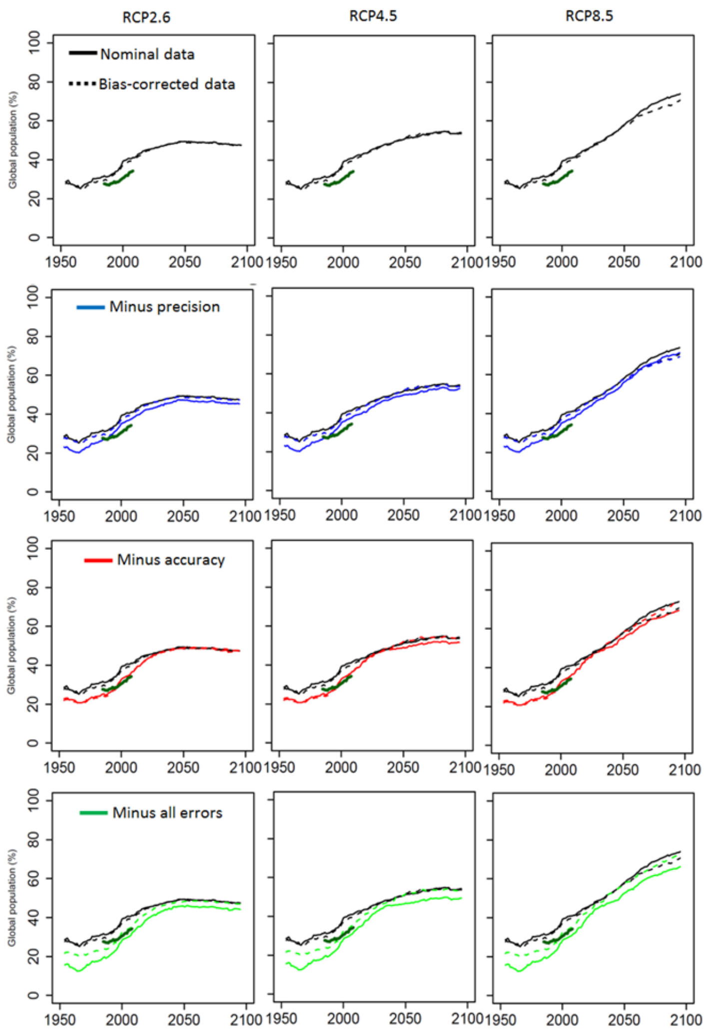

General considerations: The "accuracy" correction improved the similarity between the re-analysis and the CMIP5 data (compare red vs. dark green lines) in contrast to the direct bias correction in the climatology of temperature and relative humidity (compare straight vs. dashed lines). This suggest that the ~3% mismatch in the area of the planet (~6.4% in global population) between the reanalysis and the multimodel median is due to the treatment of the climatological bias of two variables that are related and are not independent as treated in our bias-correction test and that the "accuracy" correction is more appropriate in our case. In any case, the error in accuracy does not revert the reported trends (compare solid light-green vs. black lines).

The "accuracy" correction caused a variable effect over time despite the fact that "accuracy" is a constant. This happens because accuracy was estimated spatially (i.e., each pixel has a bias in the number of days) that is added to the simulated deadly days for that pixel, and then aggregated globally over time to generate the trend lines above. So, it is not always the case that accounting for accuracy in a given pixel will add or subtract enough deadly days in a year for that pixel to be counted in the global results shown in the trends. This variability along the accuracy trend (red lines) is larger in the human population projections, because cells affected will have different numbers of people.

E. Fischer, R. Knutti, Robust projections of combined humidity and temperature extremes. Nat. Clim. Change 3, 126 (2013)